

Microwave Model of Radiation from the Multilayer “Ocean-Atmosphere” System for Remote Sensing Studies of the Polar Regions

Vasily V. Tikhonov^{1, *}, Dmitriy Boyarskii¹, Evgene Sharkov¹, Mikhael Raev¹,
Irina Repina^{1, 2, 3}, Vladimir Ivanov⁴, Tatyana Alexeeva⁴, and Nataliya Komarova¹

Abstract—Microwave model for simulation of radiation from the multilayer system “sea surface-sea ice-snow cover-atmosphere” is introduced. In the general case, ice and snow cover is modelled by multilayer medium, where every layer is characterized by its specific physical parameters. Electrodynamical properties of each layer are determined from the original authors’ model of the effective permittivity of heterogeneous medium. This model takes into account effects of radiation scattering on irregularities of environment. Measurable physical characteristics of sea ice and snow are used as the model input data. This advantage allows using this model for interpretation of remote sensing images of the ice cover in the Polar Regions. Major attention is drawn to comparison of model calculations with satellite data and visual observations from ships. The collection of SSM/I and SSMIS images from GLOBAL-RT data base, and processed visual observations from ships in Arctic cruises were used. Observations data served as the input parameters for electro-dynamical model. Comparison of model results with SSM/I images demonstrated good coincidence at various frequencies.

1. INTRODUCTION

Ice cover is the most important climate shaping factor in Polar Regions. Existence of perennial sea ice around poles determines the state of the Earth climate system. This system is permanently changing along with changing parameters of the ice cover — area, thickness, concentration and other [1–4]. Information on ice conditions in Polar Regions is crucial for scientific and practical tasks, including monitoring of environmental changes, weather forecasting, navigation, fishery, mineral resources extraction etc..

Global monitoring of the ice cover in Polar Regions could be performed only by means of satellite-based remote sensors. The most commonly used monitoring method is passive microwave observations of the ice cover aimed on determination of spatial distribution of ice type, thickness and snow coverage [5–8].

Contemporary algorithms, used for reconstruction of the ice cover characteristics from passive microwave radiometry are typically biased due to several reasons. The largest errors emerge in summer season, in marginal ice zones and in the regions with low ice concentration [5, 9–13]. Possible routes of errors lie in the fact that these algorithms widely use empirical relationships and tuning coefficients, but sometimes miss physical processes behind.

Electrodynamical model of the system “sea surface-sea ice-snow cover-atmosphere”, introduced in this paper, was developed with respect to physical and textural parameters of the studied strata.

Received 17 February 2014, Accepted 27 March 2014, Scheduled 4 April 2014

* Corresponding author: Vasily V. Tikhonov (vtikhonov@asp.iki.rssi.ru).

¹ Department of Earth Research from Space, Space Research Institute, Russian Academy of Sciences, Profsojuznaya, 84/32, Moscow 117997, Russia. ² Air-Sea Interaction Lab, A. M. Obukhov Institute of Atmospheric Physics, Russian Academy of Sciences, Pyzhevsky Pereulok, 3, Moscow, Russia. ³ Russian State Hydrometeorological University, Malookhtinsky Prospect, 98, Saint-Petersburg, Russia.

⁴ Arctic and Antarctic Research Institute, Beringa St., 38, Saint-Petersburg 199397, Russia.

Accomplished calculations of brightness temperature satisfactorily coincide with experimental data obtained by SSM/I for the Arctic sea ice in wide range of ice concentration and snow coverage. This provides grounds for development of physically supported method targeting determination of the ice cover characteristics. Such method will improve prediction of ice conditions in the Polar Regions.

2. ELECTRODYNAMICAL MODEL

For interpretation of passive microwave data the emissivity of multilayer system is examined. The system under study consists of water and several layers of ice and snow above it. Thick air layer overlies the entire system (Figure 1).

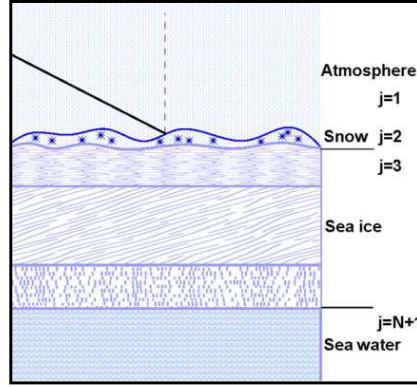


Figure 1. Model schematics.

The method, described in details in [14], was applied for brightness temperature calculations. This method was tested on the data on snow cover in the European part of the northern Russia and proved to provide successful results of SSM/I output interpretation [15]. According to this method, brightness temperature of the layered medium T_{lm} is determined from the following expressions:

$$T_{lm}^v = \sum_{j=1}^N \frac{T_j |W_j|^2}{|1 - r_j^- r_j^+ \exp(2i\psi_j)|^2} \times \left[(1 - \exp(-2\text{Im}\psi_j)) \left(1 + |r_j^- \exp(i\psi_j)|^2 \right) + 4 \frac{\text{Im}\psi_j}{\text{Re}\psi_j} \text{Re} \left(r_j^- \exp(i\psi_j) \right) \text{Im} \left(\exp(i\psi_j) \right) \times \left(\frac{|k_{zj}|^2 - k_x^2}{|k_j|^2} \right) \right] \frac{\text{Re}Z_j}{\text{Re}Z_0} + T_{N+1} |W_{N+1}|^2 \frac{\text{Re}Z_{N+1}}{\text{Re}Z_0}, \quad (1)$$

$$T_{lm}^h = \sum_{j=1}^N \frac{T_j |W_j|^2}{|1 - r_j^- r_j^+ \exp(2i\psi_j)|^2} \times \left[(1 - \exp(-2\text{Im}\psi_j)) \left(1 + |r_j^- \exp(i\psi_j)|^2 \right) + 4 \frac{\text{Im}\psi_j}{\text{Re}\psi_j} \text{Re} \left(r_j^- \exp(i\psi_j) \right) \text{Im} \left(\exp(i\psi_j) \right) \right] \frac{\text{Re}Z_j}{\text{Re}Z_0} + T_{N+1} |W_{N+1}|^2 \frac{\text{Re}Z_{N+1}}{\text{Re}Z_0}, \quad (2)$$

where subscripts v and h indicate vertical and horizontal polarizations; T_j — layer j temperature; r_j^+ , r_j^- — electric field amplitude reflection coefficients for the upper and lower boundaries of layer j , respectively; W_j — electric field amplitude transmission coefficients from the inner side of layer j upper boundary to the boundary of the medium; Z_j — wave impedance of layer of permittivity ϵ_j , $k_j = 2\pi/\lambda \times \{\sin \theta_j, 0, \cos \theta_j\} (\epsilon_j)^{1/2}$ — wave vector, $\Psi_j = k_{zj} h_j$, h_j — layer thickness. N — number of layers. Index $j = 1$ stands for the atmosphere; index $j = N + 1$ — the water surface, λ — radiation wavelength.

Measured by the sensor radiation depends on the dielectric properties of each layer, which in turn depend on layers' composition, temperature, humidity and other physical and textural characteristics. The model of multiphase disperse medium was used for determination of dielectric characteristics of ice

and snow layers. This model was successfully tested by authors for various types of snow cover, soil and ground [15–22]. According to this model, sea ice is simulated by a continuous icy medium containing spherical inclusions filled with air and brine (Figure 2(a)). Snow cover is modelled by an air medium containing spherical ice grains covered with water film and spherical drops of water (Figure 2(b)).

Dielectric properties of sea ice strongly depend on its age and meteorological conditions during ice formation. If the ice was formed under extremely low air temperature the number of air bubbles is huge. These bubbles very efficiently scatter microwave radiation. At air temperature around zero centigrade air pores in the ice start filling up with brine. Brine bubbles not just scatter electromagnetic radiation, but also absorb it. This effect is illustrated in Figure 3, where calculated relationships between scattering cross section σ_s and total cross section σ_t normalized by geometric cross section σ_g of spherical air and brine bubbles and frequency of electromagnetic radiation are shown. Calculations were carried out for typical bubble and pore sizes [23] in accordance with Mie [24] and Rayleigh [25] theories (the size of particles $\ll \lambda$).

It is important to note that dielectric properties of salt water solutions do not differ from dielectric properties of pure water at frequencies above 10 GHz [14]. This is why calculations of sections were performed for spherical water drops. As follows from the pictures, the loss of radiation on air bubbles (Figure 3(a)), incorporated in the icy medium, is caused only by scattering ($\sigma_s/\sigma_g = \sigma_t/\sigma_g$). Within the entire microwave frequency range the scattering works in accordance with Mie theory. Rayleigh scattering works only for tiny air bubbles at frequencies lower than 10–40 GHz, depending on the particle size. Water drops in the icy medium not just scatter radiation, but also intensively absorb it (Figure 3(b)). Absorption cross section σ_a could be calculated as the difference between total cross section and scattering cross section ($\sigma_a = \sigma_t - \sigma_s$) [25]. Here, as well as in almost entire microwave

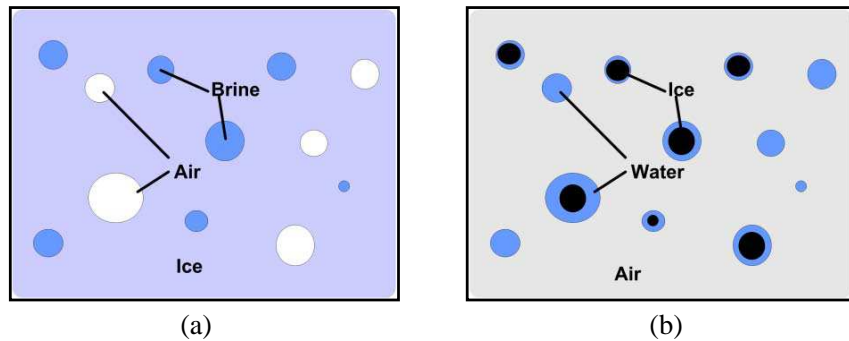


Figure 2. Model representations of (a) sea ice and (b) snow cover.

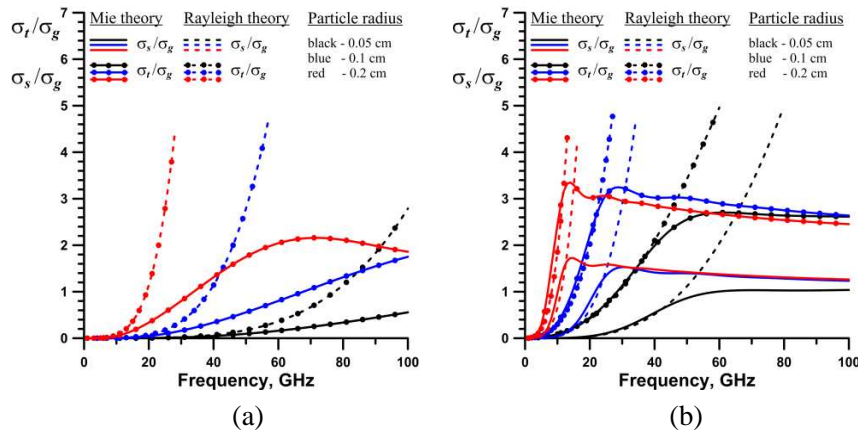


Figure 3. Scattering cross section σ_s and total cross section σ_t normalized by geometric cross section σ_g of spherical particles incorporated in the icy medium: (a) air bubbles at $t = -20^\circ\text{C}$; (b) water drops at $t = -0.1^\circ\text{C}$.

frequency range, scattering and absorption have to be calculated in accordance with Mie theory.

Snow cover on ice substantially alters radiation properties of the system “sea surface-sea ice-snow cover-atmosphere” [26–28]. When radiation penetrates through dry snow, it scatters on snow crystals. When the snow is wet, radiation is intensively absorbed. Calculated relationships between scattering cross section σ_s and total cross section σ_t normalized by geometric cross section σ_g of spherical ice particles, water drops and spherical ice grains covered with water film and frequency of electromagnetic radiation are shown in Figure 4. Calculations were done for typical size of ice seeds and water drops corresponding to fine-grained, mid-grained and large-grained snow [29–31]. The thickness of water skin around the ice seed was prescribed equal to 10% of the seed radius, corresponding to maximum relative volumetric wetness of snow (about 12%) [18, 29]. Sections calculations were also carried out in accordance with Mie theory [24] and Rayleigh [25, 32] theory (the size of particles $\ll \lambda$).

As follows from these plots, radiation loss on ice particles (Figure 4(a)) is caused by scattering only ($\sigma_s/\sigma_g \approx \sigma_t/\sigma_g$). This is explained by the fact that imaginary component of permittivity of ice in the microwave frequency range is small (< 0.01) [33]. For fine-grained and mid-grained snow Raleigh scattering is observed within almost entire frequency range. Scattering occurs in accordance with Mie theory for large-grained snow. Water drops inside snow cover (Figure 4(b)) scatter and absorb microwave radiation ($\sigma_t > \sigma_s$). Mie theory works well for water drops within almost entire frequency range, except for tiny drops (< 0.05 cm), for which Raleigh theory should be applied. Similar conclusion is also true for ice grains covered with water film (Figure 4(c)).

Scattering and absorption in ice and snow cover substantially alter dielectric properties of these mediums. This means that quantitative description of dielectric properties of ice-snow system requires taking into account scattering and absorption on structural irregularities, such as air, ice, water and brine bubbles. In accordance with selected model of dielectric properties (Figure 2(a)), effective permittivity $\varepsilon_{eff} = \varepsilon'_{eff} + i\varepsilon''_{eff}$ of sea ice could be calculated from the next formula [18, 21]:

$$\varepsilon_{eff} = \varepsilon_i \left[1 - \frac{4\pi n_a (\varepsilon_a + 2\varepsilon_i) \langle f_\omega \rangle_a}{2\varepsilon_{eff} + \varepsilon_a} - \frac{4\pi n_{sw} (\varepsilon_{sw} + 2\varepsilon_i) \langle f_\omega \rangle_{sw}}{2\varepsilon_{eff} + \varepsilon_{sw}} \right]^{-1}, \quad (3)$$

where k is wave number, n_a , and n_{sw} — concentrations of air pores and brine drops, respectively; ε_i , ε_a and ε_{sw} — permittivities of ice, air and liquid brine, respectively; $\langle f_\omega \rangle_a$ and $\langle f_\omega \rangle_{sw}$ — size-averaged amplitudes of forward scattering on air pores and brine drops, respectively.

In framework of suggested model (Figure 2(b)), effective permittivity of snow cover will be determined from the next formula [18, 21]:

$$\varepsilon_{eff}^{-1} = 1 - \frac{4\pi n_i (\varepsilon_i^w + 2) \langle f_\omega \rangle_i}{2\varepsilon_{eff} + \varepsilon_i^w} - \frac{4\pi n_w (\varepsilon_w + 2) \langle f_\omega \rangle_w}{2\varepsilon_{eff} + \varepsilon_w}, \quad (4)$$

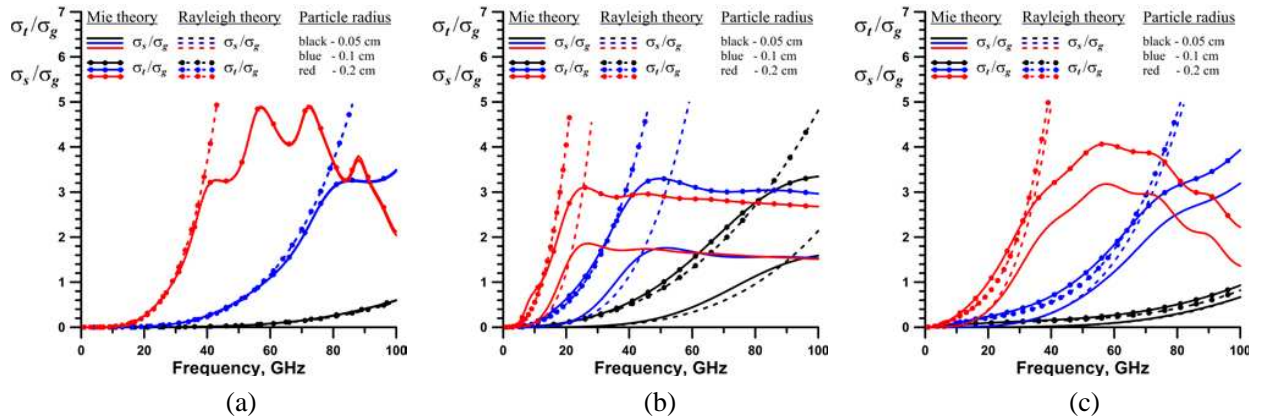


Figure 4. Scattering cross section σ_s and total cross section σ_t normalized by geometric cross section σ_g of spherical particles in the air at temperature $t = -0.1^\circ\text{C}$: (a) ice particles; (b) water drops; (c) spherical ice grains covered with water film.

where n_i and n_w are concentrations of ice grains and water drops, respectively; ε_i^w — effective permittivity of an ice grain covered with water film; ε_w — permittivity of snow; $\langle f_\omega \rangle_i$ and $\langle f_\omega \rangle_w$ — size-averaged amplitudes of forward scattering on an ice grain covered with water film and a water drop, respectively. Amplitudes of forward scattering in Expressions (3) and (4) are computed according to the Mie theory. Sizes of inclusions in sea ice and snow cover are assumed to concord with the logarithmic normal distribution law [34].

This model takes into account physical and textural features of medium as well as scattering and absorption of radiation on local irregularities. Absorption and scattering on the local irregularities (spherical particles of ice and ice grain covered with water film, air and water bubbles) in (3) and (4) are described by term f_ω , which stays for amplitudes of forward scattering on spherical particle. This relationship is explained by the forward scattering theorem, which states that total cross section σ_t , which controls radiation loss due to absorption and scattering of electromagnetic waves depends only on scattering amplitude in the forward direction [24, 25]. It is important to stress that the real particle shape is usually not spherical [23, 29–31]. However, as demonstrated in [24], particles with arbitrary shape scatter radiation in similar way as spherical particles with the same section size do, in case if the direction of scattering is close to the forward one. That is why we did not take into account specific particle shape, because this is not crucial, while the complexity of calculations would increase tremendously.

Variations of dielectric properties of sea ice and snow cover are illustrated in Figure 5. Frequency dependencies of the real and imaginary parts of permittivities are drawn for: water, solid freshwater ice, sea ice with pores filled with air, sea ice with pores filled with liquid brine, dry snow; maximum wetness snow. The curves for sea ice and snow are derived from (3) and (4), while those for water and solid freshwater ice at 0°C are taken from [33, 35]. Figure 5(a) shows that with the occurrence of air pores in ice, the imaginary part of ice permittivity drastically increases, while the real part slightly decreases. With liquid brine filling up the pores, real and imaginary parts of permittivity strongly increase, while the shape of the dependencies completely mimics that of real and imaginary parts of water permittivity. Figure 5(b) demonstrates that the effect of radiation scattering on ice grains is very important in dry snow cover. This leads to strong rise of the imaginary part of dry snow complex permittivity compared to that of solid freshwater ice. The appearance of liquid water in snow leads to a significant increase of the real and imaginary parts of wet snow permittivity, with the shape of the dependencies completely mimicking that of the real and imaginary parts of water permittivity. Actual physical properties of sea ice were used during calculations [23, 29–31].

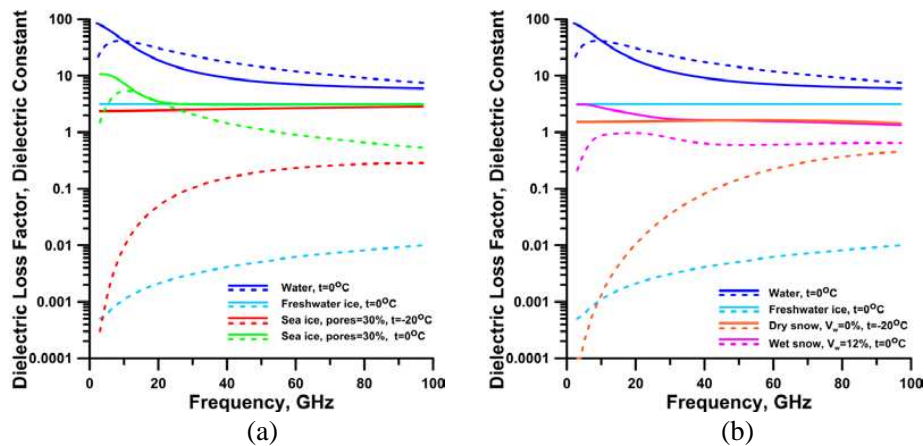


Figure 5. Frequency dependencies of the real (solid lines) and imaginary (dashed lines) parts of permittivities are drawn for: (a) water, solid freshwater ice, sea ice with pores filled with air, sea ice with pores filled with liquid brine; (b) water, solid freshwater ice, dry snow, maximum wetness snow. Parameters of sea ice: average air pores radius — 0.05 cm, dispersion of the sizes of an air pores — 40%. Parameters of a snow cover: dry snow density — 0.4 g/cm³, average ice grain radius — 0.05 cm, dispersion of the sizes of an ice grain — 40%.

Dielectric properties of sea ice and snow allow us to calculate the corresponding thicknesses of effective radiating layer (penetration depth) for microwave frequencies. The penetration depth (thickness of effectively radiating layer), that is the thickness of medium, across which the amplitude of electromagnetic wave decreases by e times, is derived from the relation [14]:

$$h = \frac{\lambda}{4\pi n''}, \quad (5)$$

where n'' is the imaginary part of complex refractive index of the medium. Figure 6 presents thickness of effectively radiating layer on microwave frequency for: snow cover, sea ice and freshwater ice. Solid curves refer to the temperature of -20°C , when no liquid phase exists either in snow or ice, dashed curves refer to 0°C , when there is the largest possible liquid phase both in snow and ice. Thin vertical lines mark SSM/I frequencies (19.35, 22.235, 37 and 85.5 GHz).

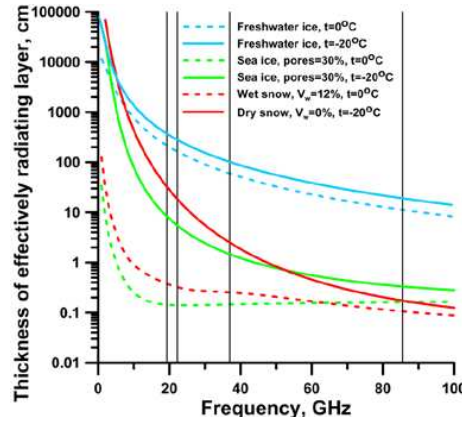


Figure 6. Frequency dependencies of the depth of radiation formation for: snow cover, sea ice and freshwater ice. Parameters of sea ice: average air pores radius — 0.05 cm, dispersion of the sizes of an air pores — 40%. Parameters of snow cover: dry snow density — 0.3 g/cm^3 , average ice grain radius — 0.05 cm, dispersion of the sizes of an ice grain — 40%.

It is clear from the Figure 6, that the thickness of effectively radiating layer is considerably smaller for sea ice than for solid ice. This is explained by stronger radiation scattering in sea ice in the presence of air bubbles as well as stronger absorption in presence of liquid brine. Hence, the imaginary part of complex refractive index of sea ice rises. The same effects (radiation scattering and absorption on impurities) determine the depth of radiation formation of snow cover. For wet snow, it is only a few centimeters for microwaves. For dry snow, it does not exceed 30 cm. Therefore, within the SSM/I frequency range, the radiation of the “sea surface-sea ice-snow cover-atmosphere” system is conditioned only by a thin upper layer of solid ground: from 20–30 cm at 19.35 GHz to a few millimeters at 85.5 GHz.

Differences in dielectric properties of sea ice and snow might cause differences in radiation characteristics of the system “sea surface-sea ice-snow cover-atmosphere” and in particular affect the brightness temperature, obtained by SSM/I sensor.

3. BRIGHTNESS TEMPERATURE OF THE SYSTEM “SEA SURFACE — SEA ICE — SNOW COVER — ATMOSPHERE”

Brightness temperature T_{br} , measured by the satellite-based radiometer was determined from the following expression, e.g., [36]:

$$T_{br} = T_1 + T_2 + T_3 + T_4, \quad (6)$$

where: T_1 is brightness temperature at the surface, reduced after passing through the atmosphere; T_2 is brightness temperature of upwelling atmospheric radiation; T_3 is brightness temperature of downwelling atmospheric radiation, reflected from the surface and reduced after passing through the atmosphere;

T_4 is brightness temperature of space radiation, reflected from the surface and reduced after passing through the atmosphere.

Standard model of the atmosphere was used in calculations [37, 38]. In framework of this model brightness temperature T_a is determined from the next formula:

$$T_a = T_X (1 - \exp(-\xi_\theta)), \tag{7}$$

where $T_X = (T_0 - 32)K$, T_0 is in situ air temperature near the surface, and ξ_θ is atmospheric absorption in the given direction. For arbitrary sampling angle, dependency of integral absorption ξ_θ on zenith angle θ in the flat stratum approximation is defined by the expression:

$$\xi_\theta = \begin{cases} \xi \sec \theta, & 0 \leq \theta < 0.4\pi \\ \xi \sec(0.4\pi) & 0.4\pi \leq \theta < \pi/2 \end{cases}, \tag{8}$$

$$\xi = \int_0^\infty \gamma(h) dh, \tag{9}$$

where $\gamma(h)$ is composed of absorption by oxygen and water vapour [37, 39].

Calculated brightness temperature of the atmosphere, measured by the satellite-based radiometer, are presented in Figure 7, which shows the sum of brightness temperature of upwelling radiation and brightness temperature of downwelling radiation reflected from the sea ice surface and reduced after passing through the atmosphere ($T_2 + T_3$). Thin vertical lines denote frequencies of SSM/I (19.35, 22.235, 37 and 85.5 GHz). This figure demonstrates that contribution of atmospheric radiation becomes important at frequencies above 35 GHz.

Brightness temperature of space radiation T_{\cos} was prescribed equal to 2.7K [39].

Taking into account Expressions (6) and (7), brightness temperature $T_{br\ lm}$ of the ice surface, which is measured by satellite-based radiometer with given polarization is expressed by:

$$T_{br\ lm} = T_{lm} \exp(-\xi_\theta) + T_a + R_{lm} T_a \exp(-\xi_\theta) + R_{lm} T_{\cos} \exp(-2\xi_\theta), \tag{10}$$

Brightness temperature of the open sea surface $T_{br\ ss}$ is expressed by:

$$T_{br\ ss} = T_{ss} \exp(-\xi_\theta) + T_a + R_{ss} T_a \exp(-\xi_\theta) + R_{ss} T_{\cos} \exp(-2\xi_\theta), \tag{11}$$

where R_{lm} and R_{ss} are reflectivities [40] of flat layered medium and flat sea surface respectively; T_{lm} is brightness temperature of the layered medium, determined from Expressions (1) or (2); T_{ss} is brightness temperature of the sea surface, which is calculated as:

$$T_{ss} = (1 - R_{ss}) T_{sw}, \tag{12}$$

where T_{sw} actual temperature of the sea surface.

Denoting the ice concentration within the radiometer scan area of by C , we get the relative square of the open water equal to $(1 - C)$. Brightness temperature, measured by radiometer T_{br} with respect to ice concentration is defined by the next expression [36]:

$$T_{br} = CT_{br\ lm} + (1 - C)T_{br\ ss}. \tag{13}$$

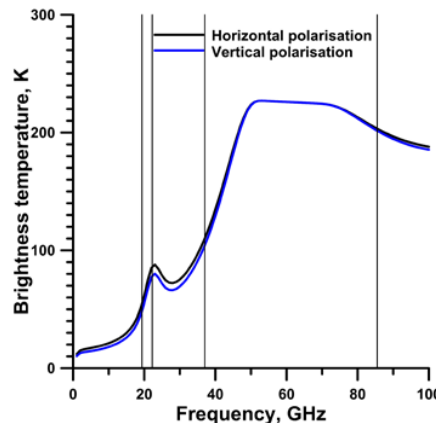


Figure 7. Brightness temperature of the upper atmospheric layers above sea ice ($T_2 + T_3$) for sampling angle equal to 53° .

For taking into account the surface roughness we used the model from [41], which defines reflectivities R_{lm} and R_{ss} , in (10)–(12) by multiplying on factor:

$$\exp(-l \cos^2 \theta), \quad (14)$$

while in Formulas (1) and (2) electric field amplitude reflection coefficients at the interface “surface-atmosphere” r_2^+ , r_1^- (see Figure 1) are multiplied on factor:

$$(\exp(-l \cos^2 \theta))^{1/2}. \quad (15)$$

Roughness parameter l is defined as:

$$l = 4\rho^2 \left(\frac{2\pi}{\lambda} \right)^2. \quad (16)$$

where ρ is square quadratic deviation of roughness at the surface.

4. DATA

Model input included the array of direct ice measurements from ships generated in Arctic and Antarctic Research Institute (AARI). These measurements were carried out onboard icebreaker “Kapitan Dranitsyn” in framework of Russian-US research project NABOS-AWLAP in the region bounded by geographical coordinates 75–85°N and 30–150°E [42]. Measurements consisted of visual determination of major ice characteristics: ice age, total ice concentration and specific ice concentration for all observed types of ice, ice shape, thickness of flat ice, snow thickness, hummocking, ice deterioration and contraction. All observations were accompanied by meteorological measurements and energy flux determination at the ice-air interface. Total ice concentration along the ship track was used for comparison of shipborn data with remote sensing measurements.

The difference in spatial resolution of shipborn and satellite data is caused by the difference in corresponding data resolutions. For comparison of satellite-based and shipborne measurements the ship track is divided into 1-km long fragments. Total ice concentration is averaged over these fragments. Resolution of satellite images SSM/I equals to 25×25 km. This means that one pixel at the image corresponds to several kilometres of ship track. In case of good visibility an observer on the bridge is able to determine total concentration over the area with radius about 8–10 km (The data obtained under bad visibility conditions were excluded from the analysis). Typical coverage by visual observations equals to 51%–64% of pixel area of the corresponding image. At the next step mean total ice concentration is estimated from visual observations for each pixel.

The data base POLE-RT-Fields, containing SSM/I and SSMIS images for Polar Regions was used. This data base was developed on the basis of GLOBAL-RT collection in the Department of Earth Research from Space, Space Research Institute RAS (SRI RAS). This data collection includes continuous measurements in 1995–2003, obtained by devices F10–F17 DMSP. Developed in SRI RAS algorithm of inter-winding and cross-apparatus equalizing and complementing allows generation of two full global radioheat Earth fields per day on the basis of band-pass data from GLOBAL-RT collection (all DMSP devices are required for filling of lacunas). Data base POLE-RT-Fields includes radio-heat fields of the Northern and Southern Earth polar caps from 85° to 60° during the time interval from 1995 till the present time at frequencies 19.35; 22.24; 37.00 and 85.5 GHz (91.655 GHz for SSMIS).

5. RESULTS

Model calculations of the Arctic ice cover brightness temperature were compared with SSM/I data (see Figure 8). Calculations were carried out in accordance with Equation (13) and Formulas (1)–(4), (7)–(12) and (14)–(16). Data array generated in AARI (see Section 4) was used for model input. Averaging over the band-pass of SSM/I device within directivity diagram of antenna was done during calculations [14]. SSM/I and SSMIS data from POLE-RT-Fields data base (see Section 4) was used for comparison. Symbols in Figure 8 denote SSM/I data, while solid lines denote model calculations. Comparisons for multiyear ice are shown in Figures 8(a)–(c), while comparisons for first year and young

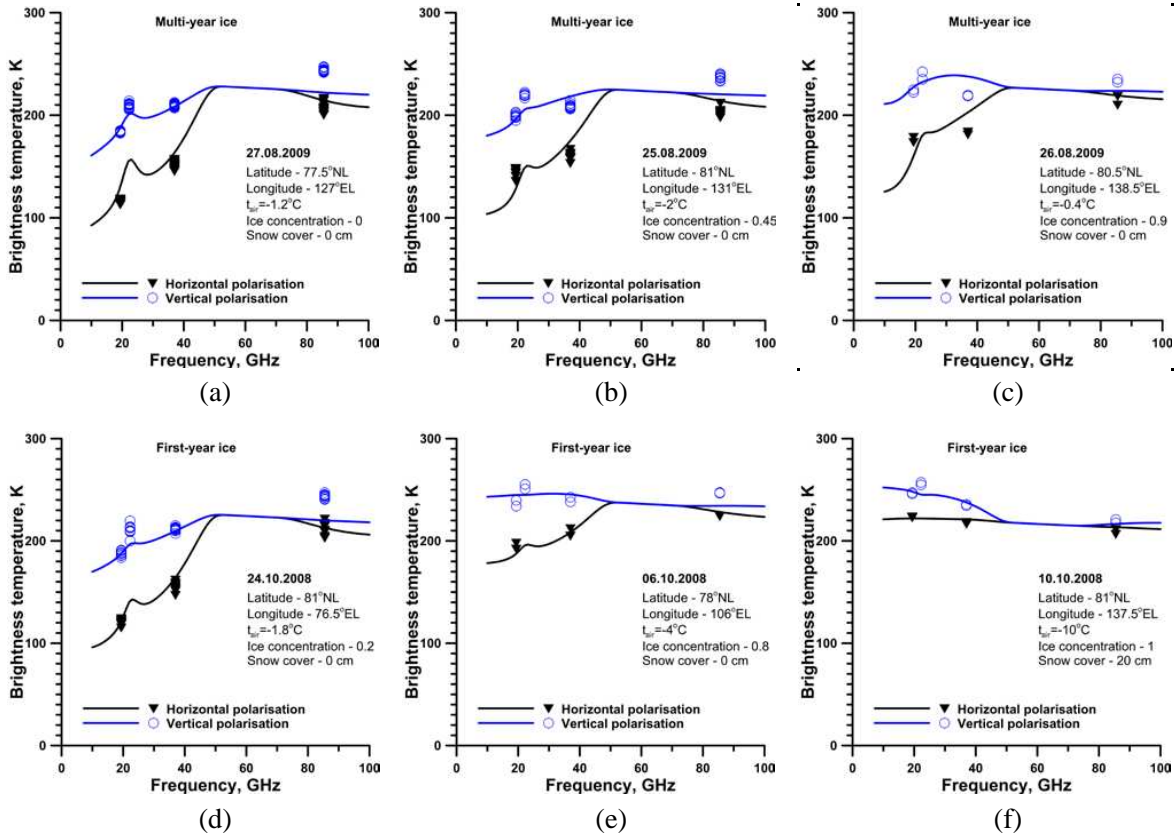


Figure 8. Frequency dependencies of brightness temperature of Arctic ice cover. Solid lines — model results, triangles and circles — SSM/I data.

ice are shown in Figures 8(d)–(f). Measurements of multiyear ice were accomplished in August 2009. Measurements of the first year ice were carried out in October 2008.

As follows from these plots, model results fit well with satellite data. Ice free water is clearly determined at frequencies 19.35 GHz and 22.235 GHz (Figures 8(a), (b), (d)). This is explained by the fact that at these frequencies real and imaginary components of permittivity reach extreme values (Figure 5), thus causing brightness temperature decrease. As we can see from figures, model results agree well with satellite data. The presence of snow cover on ice attenuates the steepness of the dependencies at 19.35 and 22.235 GHz (Figures 8(c), (f)). The thickness of the effectively radiating layer for these frequencies makes only 20–30 cm (Figure 6). Therefore, if ice is covered with a thin layer of snow, this layer gives the main contribution to brightness temperature of the “sea surface-sea ice-snow cover-atmosphere” system at frequencies higher than 10 GHz. Permittivity of snow, either wet or dry, is significantly less than that of the water or sea ice (Figure 5). This fact results in attenuation of brightness temperature dependence at lower frequencies of the given range.

6. CONCLUSION

Electrodynamic model of radiation from the ice cover, introduced in this paper, was developed with respect to physical and textural characteristics of studied mediums (ice, snow, water and air). Model calculations of brightness temperature of the Arctic sea ice with variable concentration and different snow coverage fit well with SSM/I data. Good coincidence was achieved due to taking into account textural peculiarities of ice and snow and the effects of scattering and absorption, emerging on structural irregularities within these mediums. Comparison of model calculations with SSM/I data proved the correctness of chosen approach. This provides grounds for development of method targeting determination of the ice cover characteristics in the Polar Regions on the basis of microwave radiometry.

ACKNOWLEDGMENT

The work was performed with the support of RFBR projects N 13-05-00272, 13-05-41443, 14-05-00039 and Russian Government (grant 11.G34.31.0078 “Research under supervision of the leading scientist”).

REFERENCES

1. Aagaard, K. and E. C. Carmack, “The role of sea ice and other fresh water in the arctic circulation,” *J. Geophys. Res.*, Vol. 94, No. C10, 14485–14498, 1989.
2. Barry, R. G., M. C. Serreze, J. A. Maslanik, and R. H. Preller, “The Arctic sea ice-climate system: Observations and modeling,” *Rev. Geophys.*, Vol. 31, No. 4, 397–422, 1993, Doi: 10.1029/93RG01998.
3. Vavrus, S. and S. P. Harrison, “The impact of sea-ice dynamics on the Arctic climate system,” *Climate Dyn.*, Vol. 20, Nos. 7–8, 741–757, 2003, Doi: 10.1007/s00382-003-0309-5.
4. Liu, J., J. A. Curry, and D. G. Martinson, “Interpretation of recent Antarctic sea ice variability,” *Geophys. Res. Lett.*, Vol. 31, No. 2, L02205, 2004, Doi: 10.1029/2003GL018732.
5. *Microwave Remote Sensing of Sea Ice*, F. D. Carsey, Ed., American Geophysical Union, Washington, 1992.
6. Massom, R. and D. Lubin, *Polar Remote Sensing. Volume II: Ice Sheets*, Springer-Praxis Publishing, Chichester, 2006.
7. Comiso, J., “Polar oceans from space,” *Atmospheric and Oceanographic Sciences Library*, Springer, New York, 2009.
8. Gareth Rees, W., *Remote Sensing of Snow and Ice*, Taylor & Francis Group, Boca Raton, 2006.
9. Cavalieri, D. J., K. M. St. Germain, and C. T. Swift, “Reduction of weather effects in the calculation of sea ice concentration with the DMSP SSM/I,” *Journal of Glaciology*, Vol. 41, 455–464, 1995.
10. Comiso, J. C. and R. Kwok, “Surface and radiative characteristics of the summer Arctic sea cover from multisensor satellite observations,” *J. Geophys. Res.*, Vol. 101, No. C12, 28397–28416, 1996.
11. Fetterer, F. and N. Untersteiner, “Observations of melt ponds on Arctic sea ice,” *J. Geophys. Res. — Oceans*, Vol. 103, No. C11, 24821–24835, 1998.
12. Meier, W. N., “Comparison of passive microwave ice concentration algorithm retrievals with AVHRR imagery in Arctic peripheral seas,” *IEEE Trans. Geosci. Rem. Sens.*, Vol. 43, No. 6, 1324–1337, 2005.
13. Andersen, S., R. Tonboe, L. Kaleschke, G. Heygster, and L. T. Pedersen, “Intercomparison of passive microwave sea ice concentration retrievals over the high-concentration Arctic sea ice,” *J. Geophys. Res.*, Vol. 112, No. C08004, 2007, Doi: 10.1029/2006JC003543.
14. Sharkov, E. A., *Passive Microwave Remote Sensing of the Earth: Physical Foundations*, Springer/PRAXIS, Berlin, Heidelberg, London, New York etc., 2003.
15. Tikhonov V. V., D. A. Boyarskii, L. M. Kitaev, M. D. Raev, and E. A. Cherenkova, “Regional features of microwave radiation and snow cover interaction on the example of the north of the European part of Russia,” *10th Specialist Meeting on Microwave Radiometry and Remote Sensing of Environment*, 1–4, Firenze, Italy, Mar. 11–14, 2008.
16. Boyarskii, D. A. and V. V. Tikhonov, “Microwave effective permittivity model of media of dielectric particles and applications to dry and wet snow,” *Proceeding of IEEE International Geoscience and Remote Sensing Symposium (IGARSS’ 94)*, Vol. 4, 2065–2067, Pasadena, California, USA, Aug. 8–12, 1994.
17. Tikhonov, V. V., “Model of complex dielectric constant of wet and frozen soil in the 1–40 GHz frequency range,” *Proceeding of IEEE International Geoscience and Remote Sensing Symposium (IGARSS’ 94)*, Vol. 3, 1576–1578, Pasadena, California, USA, Aug. 8–12, 1994.
18. Boyarskii, D. A., V. V. Tikhonov, N. I. Kleorin, and V. G. Mirovskii, “Inclusion of scattering losses in the models of the effective permittivity of dielectric mixtures and applications to wet snow,” *Journal of Electromagnetic Waves and Applications*, Vol. 8, No. 11, 1395–1410, 1994.

19. Tikhonov, V. V., "Dielectric and emissions models for salt water-soil mixture," *Proceeding of IEEE International Geoscience and Remote Sensing Symposium (IGARSS' 95)*, Vol. 1, 9–11, Firenze, Italy, Jul. 10–14, 1995.
20. Tikhonov, V. V., "Dielectric model of bound water in wet soils for microwave remote sensing," *Proceeding of IEEE International Geoscience and Remote Sensing Symposium (IGARSS' 97)*, Vol. 1, 1108–1110, Singapore, Aug. 4–8, 1997.
21. Boyarskii, D. A., V. V. Tikhonov, and N. Y. Komarova, "Model of dielectric constant of bound water in soil for applications of microwave remote sensing," *Progress In Electromagnetics Research*, Vol. 35, 251–270, 2001.
22. Boyarskii, D. A., V. V. Tikhonov, G. M. Chulkova, and A. R. Makavetskas, "Microwave transmission coefficient of the heterogeneous media," *Proceeding of IEEE International Geoscience and Remote Sensing Symposium (IGARSS' 03)*, Vol. 7, 4201–4203, Toulouse, France, Jul. 21–25, 2003.
23. *Sea Ice*, D. N. Thomas and G. S. Dieckmann (eds.), Wiley-Blackwell, Chichester, 2010.
24. Bohren, C. F. and D. R. Huffman, *Absorption and Scattering of Light by Small Particles*, Wiley-Interscience, New York, 1983.
25. Ishimaru, A., *Wave Propagation and Scattering in Random Media*, Academic Press, New York, 1978.
26. Comiso, J. C., T. C. Grenfell, D. L. Bell, M. A. Lange, and S. F. Ackley, "Passive microwave in situ observations of winter Weddell sea ice," *J. Geophys. Res.*, Vol. 94, No. C8, 10891–10905, 1989.
27. *Radiative Transfer Models for Microwave Radiometry*, C. Matzler (ed.), Office for Official Publications of the European Communities, Luxembourg, 2000.
28. Tikhonov, V. V., D. A. Boyarskii, I. A. Repina, M. D. Raev, E. A. Sharkov, and T. A. Alexeeva, "Snow cover effect on brightness temperature of Arctic ice fields based on SSM/I data," *PIERS Proceedings*, 514–518, Stockholm, Sweden, Aug. 12–15, 2013.
29. *Handbook of Snow*, D. M. Gray and D. H. Male, Eds., Pergamon Press, Toronto, 1986.
30. *Encyclopedia of Snow, Ice and Glaciers*, V. P. Singh, P. Singh, and U. K. Haritashya (eds.), Springer, Dordrecht, 2011.
31. Cuffey, K. M. and W. S. B. Paterson, *The Physics of Glaciers*, Elsevier, Burlington, 2010.
32. Van de Hulst, H. C., *Light Scattering by Small Particles*, John Wiley & Sons, New York, 1957.
33. Hufford, G., "A model for the complex permittivity of ice at frequencies below 1 THz", *Intern. J. Infrared and Millimeter Waves*, Vol. 12, No 7, 677–682, 1991.
34. Colbeck, S. C., "Snow metamorphism and classification," *Seasonal Snowcovers: Physics, Chemistry, Hydrology, NATO ASI Series*, Vol. 211, 1–35, 1987.
35. Ray, P. S., "Broadband complex refractive indices of ice and water," *J. Applied Optics*, Vol. 11, No. 8, 1836–1844, 1972.
36. Comiso, J. C., "SSM/I sea ice concentrations using the bootstrap algorithm," NASA Reference Publication 1380, Goddard Space Flight Center, Greenbelt, Maryland, 1995.
37. Tseitlin, N. M., *Antennas Technics and Radioastronomy*, Sov. Radio, Moscow, 1966 (in Russian).
38. Boyarskii, D. A. and V. V. Tikhonov, "The influence of stratigraphy on microwave radiation from natural snow cover," *Journal of Electromagnetic Waves and Applications*, Vol. 14, No. 9, 1265–1285, 2000.
39. Ulaby, F. T., R. K. Moor, and A. K. Fung, *Microwave Remote Sensing: Active and Passive, Volume I*, Addison-Wesley Publishing Company, Reading, 1981.
40. Born, V. and E. Wolf, *Principles of Optics*, Pergamon, Oxford, 1964.
41. Choudhury, B. J., T. J. Schmugge, A. Chang, and R. W. Newton, "Effect of surface roughness on the microwave emission from soils," *J. Geophys. Res.*, Vol. 84, No. C9, 5699–5706, 1979.
42. Polyakov, I. V., et al., "Observational program tracks Arctic ocean transition to a warmer state," *Eos, Transactions American Geophysical Union*, Vol. 88, No. 40, 398–399, 2007.